# Electrochemical Deactivation of Switchable Catechol-Containing Smart Adhesive from Nonconductive Surfaces

Md Saleh Akram Bhuiyan, James Manuel, Fatemeh Razaviamri, Bruce P. Lee\*

Department of Biomedical Engineering, Michigan Technological University, Houghton,

Michigan 49931, United States

KEYWORDS: Catechol-containing adhesive, *In situ* deactivation, Nonconductive surface, Electrochemical oxidation, Lap shear test, Electrochemical reversibility

#### ABSTRACT

The feasibility of deactivating and reactivating catechol-containing smart adhesive electrochemically while in direct contact with a nonconductive surface was explored in this work.

The adhesive was coated over an aluminum mesh-attached polydimethylsiloxane (AM-PDMS) substrate. The aluminum mesh served as an electrode to apply electricity through the adhesive. A silver (Ag) counter electrode was coated in the periphery of the adhesive-substrate interface to

deactivate the adhesive attached to the nonconductive surfaces including glass and poly(methl methacrylate) (PMMA) substrates. The deactivation of adhesive was performed with the application of up to 20 V of applied electricity utilizing the Ag electrode as a cathode and aluminum mesh as an anode. The adhesion strength of adhesive towards nonconductive surfaces decreased by 98% after in situ application of electricity. The deactivation rate was tunable with the applied voltage level, exposure time to applied voltage, surface area of the adhesive interface, and aluminum mesh size. The deactivated adhesive was reactivated electrochemically by reversing the electrode polarity up to 3 cycles utilizing catechol-boronate complexation chemistry.

## INTRODUCTION

A smart adhesive can be deactivated or reactivated in response to externally applied stimuli (e.g., pH, temperature, light), which has various applications in multiple fields (e.g., biomedical, structural joints, automotive industry, robotics)<sup>1-5</sup>. However, most of the existing smart adhesives exhibit poor adhesion in a wet environment<sup>6</sup>. Recently, smart adhesives inspired by mussel adhesive proteins containing catechol have been developed for their ability to bond to wet surfaces reversibly<sup>7, 8</sup>. The interfacial binding of catechol to various surfaces is often based on H-bonding, electrostatic interaction, and coordination bonds<sup>9-13</sup>. The adhesive property of catechol is

dependent on its oxidation state, which can be controlled by changing pH<sup>14-16</sup>. Previously, we demonstrated that it is feasible to directly deactivate surface-bound catechol-based adhesive through electrochemical oxidation of catechol<sup>17, 18</sup>. Our works inspired Huang et al.<sup>19</sup> to design a climbing robot that utilized catechol-containing hydrogels as adhesive pads and electrical current was utilized to control the adhesive property of the hydrogel. However, these existing designs relied on a conductive surface to function as a counter electrode<sup>17-19</sup>, which greatly limit the application of catechol-based smart adhesives. Therefore, the ability to deactivate catechol-based adhesive while it is bound to a nonconductive surface needs to be explored.

The reduced form of catechol exhibits strong adhesion under acidic conditions but oxidizes in a basic pH with poor adhesive property<sup>13</sup>. This pH-responsive chemistry can be controlled through electrochemical oxidation and reduction of catechol initiated by a two-electrode (anode and cathode) system in the presence of water<sup>17-19</sup>. Water electrolysis begins with the application of electricity, resulting in a basic pH surrounding the cathode<sup>20</sup>. Therefore, when catechol-based adhesive is exposed to the cathode, it oxidizes irreversibly and demonstrates weak adhesion. The irreversible oxidation of catechol can be prevented by adding a temporary protecting group, such as boronic acid<sup>14, 16, 17</sup>. This protecting group forms a complex with catechol at basic pH that

generates near the cathode and the complex is also poorly adhesive<sup>17</sup>. Breaking the catechol-boronate complex in an acidic media<sup>14, 16, 17</sup> or by reversing the polarity of the cathode to an anode<sup>19</sup> re-expose the catechol for strong adhesion. Therefore, using two electrodes across the adhesive and controlling their polarity is essential to achieve electrochemically reversible adhesion of catechol. Furthermore, the electrode area also plays a vital role in controlling the extent of water electrolysis responsible for electrochemical deactivation and reactivation of adhesives<sup>21</sup>. Hence, positioning electrodes across the adhesive becomes challenging to design for electrochemical deactivation, followed by reversible adhesion of an adhesive in direct contact with a nonconductive surface.

Here, we demonstrated the feasibility of controlling the adhesion of a catechol using *in situ* electrochemistry when the adhesive is bound to a nonconductive surface. The adhesive was polymerized over an aluminum mesh (AM) attached in a polydimethylsiloxane (PDMS) substrate, where the metal mesh served as an electrode. A silver (Ag) electrode was fabricated on the nonconductive surface as the counter electrode, where the Ag electrode was coated around the periphery of the adhesive joint. This configuration enabled us to achieve *in situ* deactivation of adhesive in direct contact with a nonconductive surface by applying electricity directly to the

adhesive using lap shear test setup. The effect of the level of applied voltage, exposure time of the applied voltage, the area of the adhesive interface, and mesh size on the extent of adhesive deactivation was investigated. Finally, the reversible nature of the adhesive was explored by incorporating phenylboronic acid as the protecting group into the adhesive formulation and the polarity of the two electrodes were reversed to reactivate the adhesive.

## MATERIALS AND METHODS

## Materials

Methoxyethyl acrylate (MEA), 3-(trimethoxysilyl)propyl methacrylate (TMSPMA), acrylic acid (AAc), 3-(acrylamido)phenylboronic acid (APBA), silicon oil, dimethyl sulfoxide (DMSO), and dimethyl sulfoxide-d6 (DMSO-d6) were purchased from Sigma-Aldrich (St. Louis, MO). Methylene bis-acrylamide (MBAA) and 2,2-dimethoxy-2-phenylacetophenone (DMPA) were purchased from Acros Organics (New Jersey). Dimethylformamide (DMF), diethyl ether, hydrochloric acid (HCl), quartz glass, and ethanol were purchased from Fisher Scientific (Fair Lawn, NJ). 2,2'-Azobis(isobutyronitrile) (AIBN) was purchased from Wako Pure Chemical Industries, Ltd. (Osaka, Japan). High-strength grade 5 titanium (Ti surface (Ti6Al4V)) or sheet, 0.016" thick × 6" wide ×6"long), aluminum wire cloth (8 × 8/16 × 16 mesh size, 0.097"/0.045"

opening size, 60%/51% open area, 0.028"/0.018" wire diameter, respectively), ultra-chemicalresistant poly(tetrafluoroethylene) (PTFE) sheet (1/6" thick), clear scratch- and UV-resistant cast poly(methl methacrylate) (PMMA) sheet (1/16" thick), mirrorlike multipurpose 110 copper wire (0.003" diameter), clear impact-resistant polycarbonate sheets (1/4" thick), high-strength hightemperature silicone rubber sheet with adhesive-back (Red, 5 mm thick), borosilicate glass sheet (3" x 3", 1/4" thick), and 200 g test weight were purchased from McMaster-Carr (Elmhurst, IL). Sylgard 184 silicone elastomer was purchased from Dow corning (Midland, MI). Dopamine methacrylamide (DMA) and an acidic solution (pH 3) were prepared following previously published protocols<sup>18</sup>. In brief, the pH 3 solution was prepared in the lab by titrating 1 M hydrochloric acid (HCl) into a mixture of 1 L deionized (DI) water and 0.1 M sodium chloride (NaCl).

# Preparation of Adhesive-coated AM-attached PDMS (AM-PDMS)

Adhesive-coated AM-PDMS was prepared by attaching an aluminum mesh onto the surface of PDMS followed by *in situ* polymerization of catechol-containing adhesive over AM-PDMS. PDMS base and crosslinking agent mixture (10:1) was poured inside a cavity (1 inch  $\times$  1 inch) created by compressing a PTFE mold (thickness of  $\approx$ 3.5 mm) on a glass surface (**Figure S1**). The

mixture was partially cured for 54 min at 60 °C. The PTFE mold was removed, leaving the partially crosslinked PDMS on the glass surface. An aluminum mesh (mesh size =  $8\times8$  or  $16\times16$ ) was then attached to the top of the PDMS surface and compressed with a hard polycarbonate mold (thickness 5 mm) using binder clips and kept at 60 °C for 2 hours. Meshes with mesh sizes of  $8\times8$  and  $16\times16$  contains 8 and 16 openings, respectively, within a 1-inch square area. The prepared sample was stored in a closed container until the next step.

To covalently link the adhesive coating onto the surface of AM-PDMS, AM-PDMS was functionalized with a polymerizable methacrylate group, 3-(trimethoxysilyl)propyl methacrylate (TMSPMA) (Scheme 1), following a previously published protocol<sup>22</sup>. The surface of AM-PDMS was treated with oxygen plasma (200 W and 200 mTorr) for 5 min (Trion technology Phantom II, Clearwater, FL). Then, the substrate was transferred immediately into a mixture of deionized (DI) water and ethanol (1:1) containing 4 vol% of TMSPMA. The TMSPMA-functionalized AM-PDMS was kept in this mixture for one hour with gentle nutation. After one hour, the substrate was washed with DI water, dried with nitrogen, and kept inside a closed container until the next step.

**Scheme 1**. Preparation of adhesive-coated AM-PDMS.  $I = R_1 = DMA$ ,  $II = R_2 = MEA$ , III = MBAA, IV = R4 = APBA, V = p(DMA-co-MEA-co-AAc), and  $R_3 = AAc$ . The complete chemical

structure of the copolymer is shown in figure S2. The AAc in the copolymer can simultaneously interact with catechol, MEA, and boronic acid<sup>23</sup> present in the adhesive.

To ensure that the adhesive was chemically linked to the TMSPMA-functionalized AM-PDMS, 100 µL of 0.1 mol% DMPA solution in ethanol was first added on top of the substrate, which was then dried under a stream of nitrogen. TMSPMA-functionalized AM-PDMS was placed inside a mold consisted of a silicone rubber enclosure (5 mm thick,  $1.5 \times 1.2 \times 0.2$  inches) attached to a glass slide (Figure S2). A precursor solution was prepared by dissolving MEA (3.0 mmol), DMA (1.6 mmol), MBAA (0.16 mmol), and DMPA (0.004 mmol) in 2.5 mL of DMSO. Separately, a solution containing a linear copolymer of p(DMA-co-MEA-co-AAc) (Figure S3) was prepared by dissolving 130 mg of the copolymer in 1 ml of DMSO. p(DMA-co-MEA-co-AAc) was synthesized using AIBN-initiated polymerization of a solution containing MEA (0.514 mL, 4 mmol), DMA (88.4 mg, 0.4 mmol), and AAc (14.5 mg, 0.2 mmol) and AIBN (20 mg, 0.12 mmol) dissolved in DMF (5 ml) at 60 °C for 24 h followed by precipitation in diethyl ether. A mixture containing the precursor solution and p(DMA-co-MEA-co-AAc) solution was prepared with a weight ratio of 75:25 between MEA and the copolymer. The entire mixture was purged with nitrogen and stirred for 1 hr. 3.3 ml of precursor-copolymer mixture was added over TMSPMAfunctionalized AM-PDMS and polymerized for 40 min in a UV cross-linking chamber (XL-1000,
Spectronics Corporation; Westbury, NY) located in a nitrogen-filled glovebox (PLAS
LABORATORIES; Lansing, MI). The adhesive-coated AM-PDMS was washed 3 times with pH
3 solution and incubated in pH 3 for 1 hour before testing to obtain the reduced form of catechol.
To prepare an adhesive that could be reactivated, 1.6 mmol phenylboronic acid (APBA) was added
to the precursor solution and the adhesive was prepared as described above.

## Preparation of Ag electrode on Nonconductive Surface

Ag electrode was prepared by mixing a two-part epoxy adhesive containing 60% Ag particles by weight and applied it onto a glass slide or a PMMA sheet (2 inch × 1 inch) (**Figure S4**). The area (300 or 150 mm<sup>2</sup>) where the adhesive will come into contact with the substrate was first covered by a Ti sheet. Next, the epoxy adhesive mixture was painted at the edge of the sheet. After removing the sheet and waiting for 10 min, a second layer of the epoxy adhesive mixture was painted over the coated electrode to seal the pinholes that may have formed during the curing process. The thickness of the electrode was measured using a Filmetrics 3D Profilometer. The

dimension of the Ag electrode was adjusted to fit around adhesive-surface interface so that the Ag electrode is located immediately adjacent to the adhesive joint.

#### **Lap Shear Adhesion Test**

Lap shear adhesion test (**Figure 1**) was performed using a universal testing machine (UTM; MTS Acumen 3, ±3kN, MTS Systems Corporation, Eden Prairie, MN). A typical lap shear bond was formed in a pH 3 buffer between the adhesive-coated AM-PDMS and plasma treated (15 W, 140 mTorr, 1 min) surface with an overlapped surface area of 300 or 150 mm<sup>2</sup>. A 200 g weight was placed over the adhesive joint for 30 min to obtain a stable attachment. Then, the lap shear test was performed following ASTM D5868. The adhesion strength was evaluated by following the equation below.

Adhesion strength = 
$$\frac{Maximum\ adhesive\ force\ (N)}{Area\ of\ lap\ shear\ bond\ (mm^2)}$$
 x 1000 kPa [Equation 1]

To evaluate the ability to deactivate and reactivate the surface-bound adhesive *in situ*, a power source (Keithley 2460 Source Meter) was connected to the AM and Ag electrodes. To deactivate an adhesive in direct contact with a nonconductive surface, adhesive joint was formed by positioning the Ag electrode around the periphery of the adhesive, so that the interfacial bond was formed between the adhesive and the surface substrate. The adhesive joint was loaded into the

UTM using two clamps, where the clamp's inner surface was covered with nonconductive tape to avoid an electrical short circuit between the power source and UTM during electrical application. Then, a voltage ranging from 10-20 V was applied for up to 4 min, and the power source recorded the current flow through the adhesive. The samples were then pulled to failure immediately after the application of electricity. For comparison purposes, a conductive Ti surface was used, and electricity was applied without the Ag electrode. To reactivate the adhesive, the deactivated samples were exposed to electricity with reversed polarity of the electrodes prior to adhesion testing.

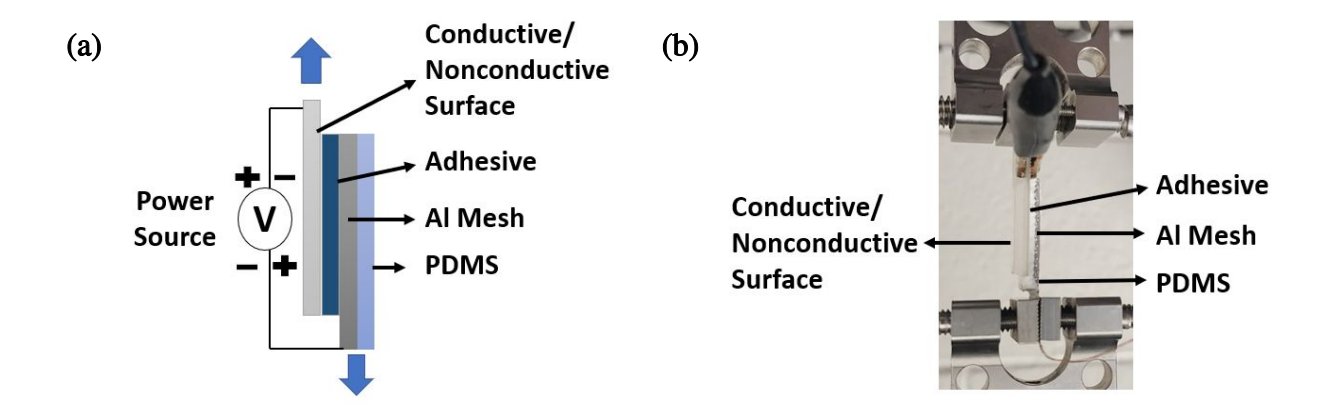


**Figure 1.** (a) Schematic representation and (b) photograph of lap shear test setup used for adhesion testing during in situ application of electricity.

#### **Characterization of Adhesive Surface**

The surface roughness of the deactivated adhesive was measured by scanning  $800 \times 800 \ \mu m^2$  area using a Filmetrics 3D profilometer. The roughness value was reported as average roughness (Sa)

and root mean square roughness  $(Sq)^{24, 25}$ . The stiffness of the adhesive surface was assessed via determining Young's modulus of the adhesive at interface ( $E_{inf}$ ) by following previously published protocol<sup>18</sup>. In brief, Ti sphere was brought into contact with the adhesive at 1 µm/s until a maximum preload of 10 mN was reached. The force (F) vs. displacement ( $\delta$ ) curve was fitted with the Hertzian model<sup>26</sup> to determine  $E_{inf}$  as shown in the following equation,

$$\mathbf{F} = \frac{16R^{1/2}E_{inf}\delta^{3/2}}{9}$$
 [Equation 2],

where R is the radius of curvature of the Ti sphere.

# **Statistical Analysis**

SigmaPlot was used to perform statistical analysis. One-way analysis of variance (ANOVA) with the Tukey method and Student's t-test was used for comparing multiple and two groups, respectively, using a p value of 0.05.

# RESULTS AND DISCUSSION

## **Preparation of the Adhesive-coated AM-PDMS:**

The catechol-containing adhesive used in this study was polymerized over a TMSPMA-modified AM-PDMS through UV-initiated free-radical polymerization. During the process of creating AM-PDMS, AM was pressed over partially cured PDMS, which created millimeter-sized circular bumps on the surface PDMS (Figure 2). From the cross-sectional image, although AM was attached within the PDMS substrate, Al wires were still exposed to the adhesive. These

exposed wires of the mesh were necessary to directly conduct electricity to the adhesive coating due to the poor conductivity of PDMS. The surface of the adhesive coating was flat and the average thickness of the adhesive on the AM-PDMS substrate was around 2 mm.

During the adhesive coating process, ATR-FTIR was used to confirm chemical functionalization during each coating step (Figure S5). The TMSPMA-coated AM-PDMS exhibited characteristic peaks of C=C at 1642 cm<sup>-1</sup> and C=O at 1733 cm<sup>-1</sup> to indicate the successful modification of TMSPMA<sup>22, 27</sup>. The methacrylate in TMSPMA undergoes free radical polymerization with the monomers found in the precursor solution so that the UV-cured adhesive can be covalently linked to the PDMS surface. ATR-FTIR spectra of the adhesive coating confirmed the presence of MEA (C=O 1732 cm<sup>-1</sup> and C-H stretch 2689-3026 cm<sup>-1</sup>) and catechol (-OH peak near 3387 cm<sup>-1</sup>, out-ofplane C-H bending of the benzene ring at 709 cm<sup>-1</sup>)<sup>18</sup>. Adhesive were further formulated with a p(DMA-co-MEA-co-AAc) which consist of 8.5 and 4.5 mol% of DMA and AAc, respectively, based on <sup>1</sup>H NMR (Figure S6). p(DMA-co-MEA-co-AAc) was added to the adhesive to form an semi-interpenetrated network (S-IPN)-like structure to enhance intermolecular interaction within the bulk of the adhesive matrix<sup>23</sup>. FTIR spectra of copolymer-incorporated adhesive exhibited an increased peak intensity at 1732 cm<sup>-1</sup> corresponding to the of C=O of AAc from the copolymer.<sup>28</sup>

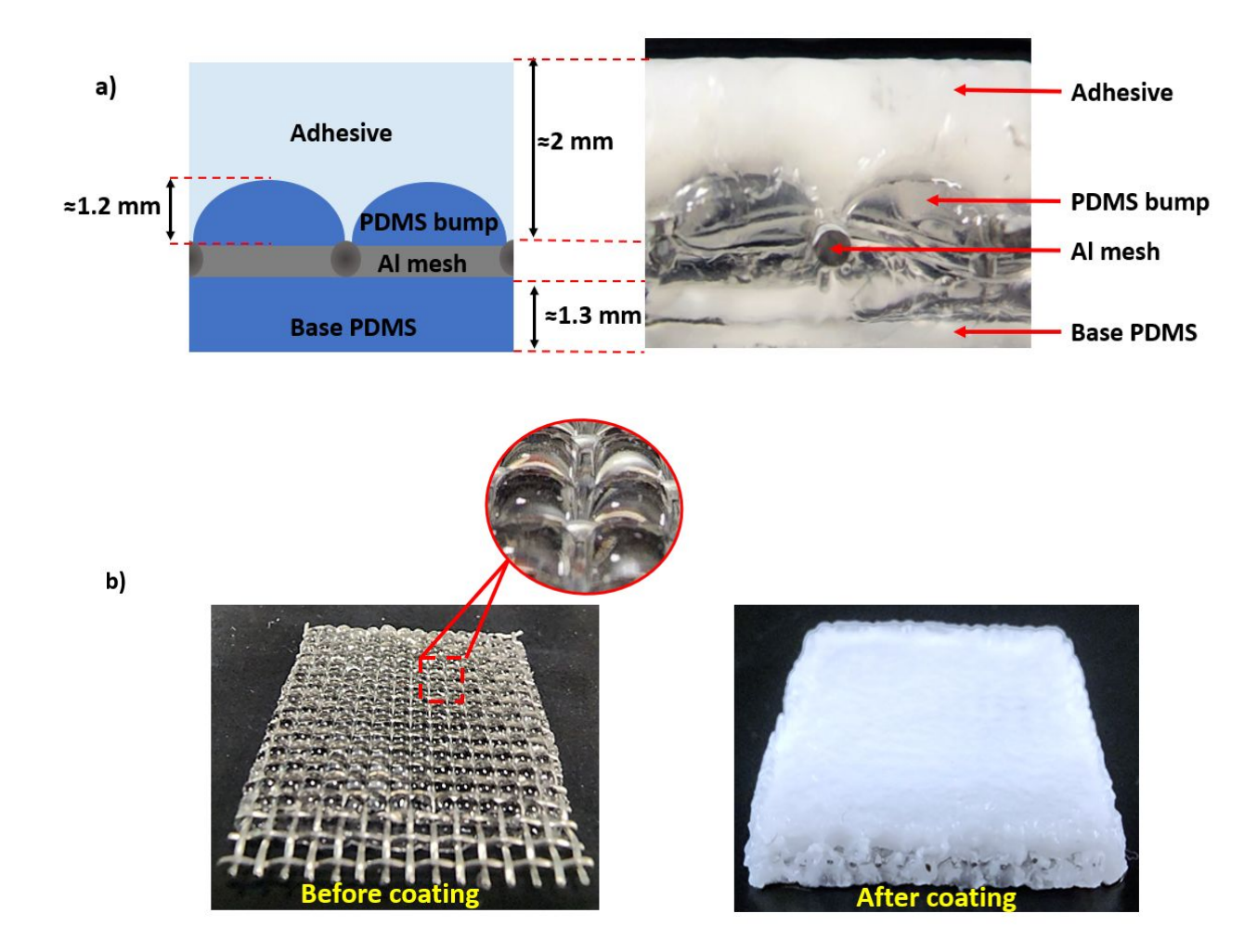


**Figure 2.** (a) Schematic representation (left) and photograph (right) of the cross-sectional view of adhesive-coated AM-PDMS. (b) Photographs of AM-PDMS before (left) and after (right) coating with an adhesive. The inset shows the zoomed view of the millimeter-sized circular surface, which is not visible after coating the substrate with the adhesive. AM mesh size is  $16\times16$ .

# **Adhesion Property before Exposure to Applied Electricity:**

Lap shear adhesion test was performed to evaluate the adhesive property of adhesive-coated AM-PDMS in the absence of applied electricity. The typical adhesive used in these experiments was prepared on a 16×16 AM-PDMS that contained 40 wt% of catechol relative to the MEA with an adhesive overlapping area of 300 mm<sup>2</sup>. The adhesive demonstrated strong adhesion to nonconductive glass and PMMA surfaces as well as conductive Ti surfaces (Figure 3). The adhesion strength towards glass and Ti surfaces was around ≈ 40 kPa. Catechol can interact with glass through H-bonding<sup>9</sup> and Ti through monodentate or bidentate coordination bonds<sup>12</sup>. Moreover, catechol can also interact with PMMA surface through H-bonding<sup>29</sup>. However, the adhesion strength towards the PMMA surface was slightly lower (30 kPa). A similar trend was found in a previously published study<sup>30</sup>. The contributions of other parameters on the measured adhesion strength were also evaluated. Lap shear adhesion strength increased with increasing catechol content and the formulation that did not contain catechol did not demonstrate measurable adhesive property (Figure S7). Incorporation of p(DMA-co-MEA-co-AAc) also contributed to increased adhesive property (Figure S8). The formation of hydrogen bonds between AAc and the MEA and catechol of the adhesive network likely increased the toughness of the coated adhesive<sup>31</sup>- <sup>34</sup>. This increased toughness of the adhesive contributed to the increased adhesion strength towards the Ti surface<sup>35, 36</sup>.

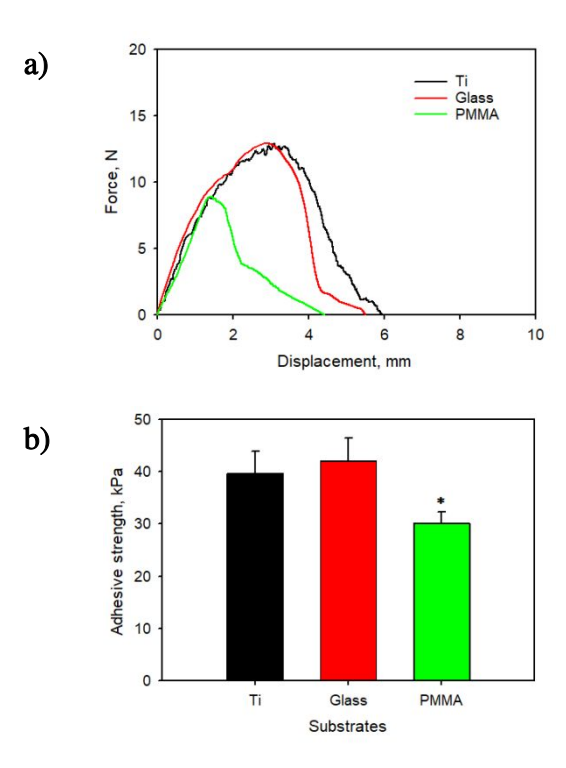


Figure 3. (a) Lap shear curve, and (b) adhesion strength of the adhesives tested with various interacting surfaces. The adhesives were prepared on  $16\times16$  AM-PDMS, and the area of the adhesive interface was  $300 \text{ mm}^2$  in these experiments. \* p < 0.05 when compared to the adhesive tested with different interacting surfaces. (n = 3)

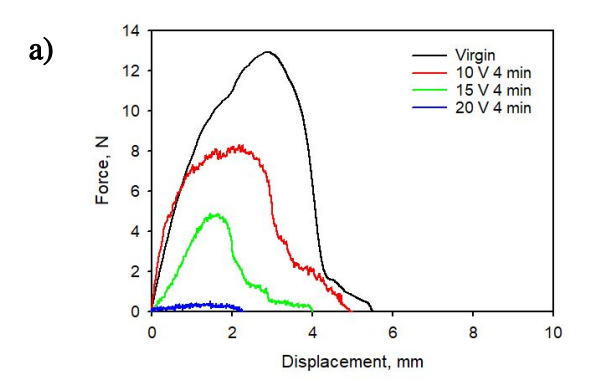
The effect of mesh geometry on the adhesive strength was also explored using 30×30, 16×16, and 8×8 mesh sizes (**Figure S9**). The prepared substrate revealed the different sizes of PDMS

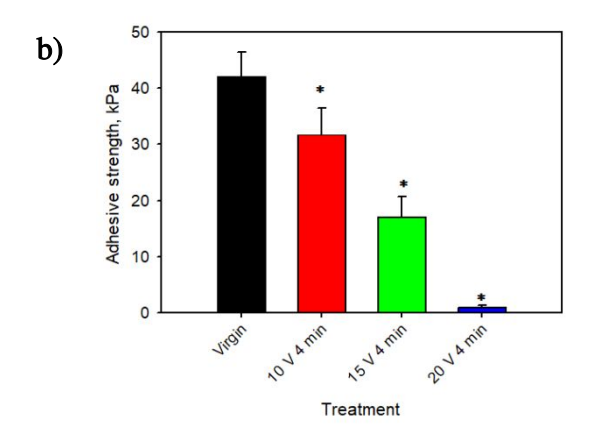
bumps based on the mesh size. The substrate prepared with 8×8 mesh had bigger PDMS bumps compared to the substrate with 30×30 mesh. After coating these substrates with the adhesive, 30×30 AM-PDMS-containing adhesive exhibited lower adhesion strength than the others. We believe that the S-IPN-like adhesive, PDMS bumps, aluminum mesh, and base PDMS layer of the substrate play a critical role in controlling the adhesive performance by dissipating energy into the adhesive and PDMS <sup>35, 37, 38</sup>. Hence, the adhesion strength improved while using 16×16 AM-PDMS. However, the diameter and rigidity of the mesh increased with increasing mesh size, which can counteract the energy-dissipating mechanism. Therefore, the adhesion strength did not improve further using the 8×8 AM-PDMS substrate.

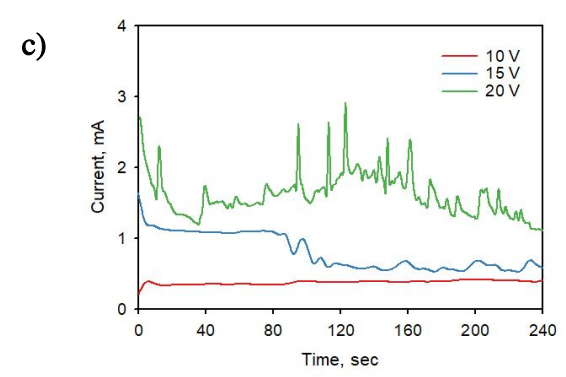
# Deactivation of Adhesive from Nonconductive Surface:

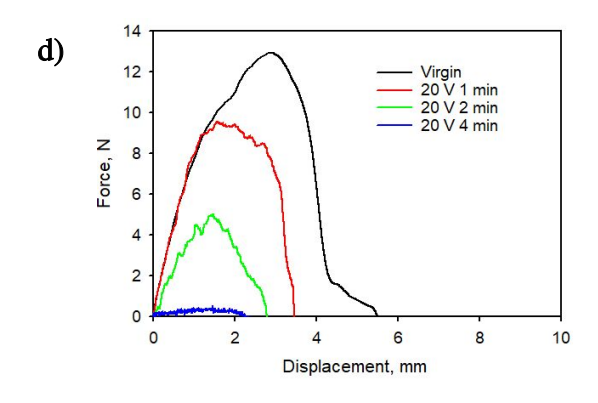
To deactivate the adhesive from a nonconductive glass surface, an adhesive interface was formed between the adhesive and a glass surface containing an Ag electrode (**Figure S10**). The thickness of the Ag electrode was around 700  $\mu$ m. Once the adhesive joint was formed, the electrode is positioned around the periphery of the adhesive to create a close proximity between the adhesive and the electrode for providing an electrical path during electrochemical oxidation. An electrical potential of 10-20 V was applied using the Ag electrode as the cathode and AM as the anode.

Adhesion strength decreased with increased applied voltage (**Figure 4**). As expected, the current recorded *in situ* also increased with increasing level of applied voltage. Fluctuation of the current level was observed due to the oxygen and hydrogen bubbles generated by water electrolysis<sup>39, 40</sup>. Similar results were also observed in our previously published studies<sup>17, 18</sup>. However, the adhesive strength was reduced by 98% when 20 V was applied for 4 min when compared to the virgin adhesive. Similarly, adhesion strength also decreased with an increased exposure time (**Figure 4d and e**). The Sa and Sq roughness of the adhesive was around 0.6 - 0.8 µm and there was no significant change after deactivation (**Figure S11**). On the other hand, the stiffness of the adhesive surface increased after applied electricity (**Figure S12**). This result may be attributed to catechol oxidation and crosslinking resulting in the formation of a stiffener network<sup>18</sup>.









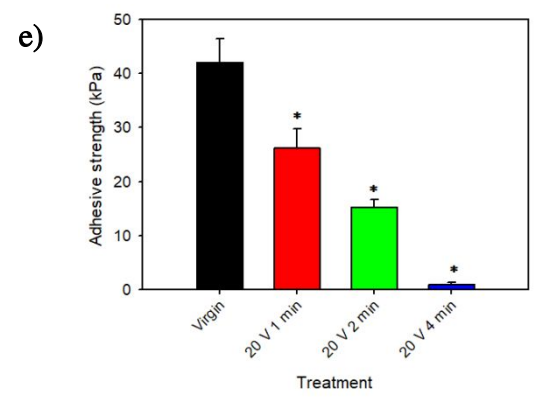


Figure 4. (a) Force vs. displacement curve, (b) adhesion strength, and (c) recorded current for adhesive adhere to a glass surface with different levels of applied voltage for 4 min. (d) Force vs. displacement curve and (e) adhesion strength of adhesive when exposed to 20 V for up to 4 min. The electricity was applied using cathodic AM and anodic Ag electrodes. The adhesive contained 40 wt% of catechol relative to the MEA. The adhesives were prepared on  $16 \times 16$  AM-PDMS substrates. The area of the adhesive interface was  $300 \text{ mm}^2$  in these experiments. \*p < 0.05 when compared to the virgin adhesive. (n = 3)

The supplementary **Videos S1** and **S2** captured the deactivation process of the adhesive from a glass surface weighted with a mass of 200 g. The adhesive detached from the glass surface at 2 min 10 sec, (**Video S1**). The adhesive detached due to the reduction of the adhesion strength to the extent that the adhesive could no longer carry the weight attached to it. When viewing the adhesive joint through the glass surface, cracks in the interfaced formed near the edges of the adhesive joint almost immediately when electricity was applied (**Video S2**). These cracks propagated toward the center of the adhesive joint and finally led to the complete detachment of the adhesive around 2 min.

The adhesion strength decreased after applying the electrical field due to the oxidation of catechol at the adhesive interface<sup>18</sup>. The oxidized catechol appeared red in color, which is visible on the surface of the detached adhesive after deactivation (**Figure S13**). The red color was more

intense near the Ag cathode along the edges of the adhesive, indicating that the extent of catechol oxidation was higher in these areas. Correspondingly, the pH near these regions was also more basic (pH 7-8) when compared to the central region of the adhesive (pH 5-6) (**Figure S14**). The application of electricity potentially initiated water electrolysis, which increased the pH near the cathode and induced catechol oxidation. To verify the change in pH at the interface, phenol red, a pH indicator, was added to the adhesive during deactivation (**Video S3**). The water at the interface turned red, indicating a shift in the pH of interfacial liquid to a basic pH.

When the contacting area at the interface was reduced from 300 mm² to 150 mm², the adhesive was deactivated at a faster rate (Figure S15). For adhesive with an interfacial area of 150 mm², the adhesive strength decreased linearly at a rate of 19.2 kPa/min (Table S1). On the other hand, the rate of decrease for adhesive with an interfacial area of 300 mm² was much lower (< 15 kPa/min). The red coloration associated with the oxidation of catechol appeared throughout the entire surface of the 150 mm² adhesive (Figure S15c) rather than an intense discoloration near the cathode for 300 mm² adhesive (Figure S14). Additionally, an increased current level was recorded while deactivating the adhesive (4-5 mA for 150 mm², Figures S15d) compared to the current level observed while deactivating the adhesive with a 300 mm² interface (~2 mA; Figure 4c). The pH of

the interfacial liquid was also found to be more basic for the smaller interfacial area (Figure S16). These results collectively indicated the rate of deactivation increased with decreasing surface area at the interface. For a smaller interfacial area, any given portion of the adhesive is located closer to the counter electrode when compared to that of an adhesive with a larger surface area. As such, it resulted in a larger change in local pH gradient and more complete and uniform catechol oxidation. Most importantly, the electrical resistance for the smaller adhesive was also lower, which facilitated faster deactivation.

Similarly, an adhesive coated onto an  $8\times8$  AM-PDMS demonstrated significant higher reduction in adhesion strength when compared to adhesive coated on a  $16\times16$  AM-PDMS (**Figure S17**). Wire diameter for  $8\times8$  AM (diameter = 0.028'') was significantly higher when compared to that of the  $16\times16$  AM (diameter = 0.018''), which resulted in a significant increase in the level of recorded electrical current<sup>41,42</sup>. These results collectively indicated that the level of electrical current passing through the adhesive interface has a significant impact on the rate of adhesive deactivation.

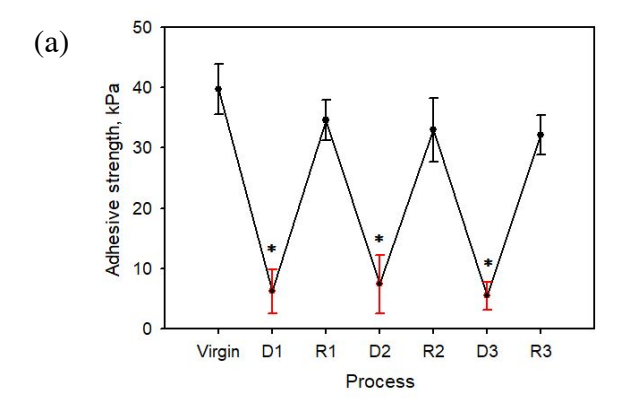
In addition to glass surface, catechol-containing adhesive also successfully deactivated from a polymeric and nonconductive PMMA surface (**Figure S18**). The time it took to completely deactivate the adhesive was similar to that obtained for the glass surface. However, it took only 90

sec to deactivate the adhesive bound to a conductive Ti surface (**Figure S19**). Using a conductive material as an interacting surface eliminated the need of the Ag electrode. In addition, the entire area of the conductive (Ti) surface served as a cathode (300 mm<sup>2</sup>) to apply electricity directly to the adhesive (**Scheme S1**). On the contrary, the inner periphery of the Ag cathode was only available to apply electricity to the adhesive for deactivating it from the nonconductive glass and PMMA surfaces. As such, deactivating the adhesive from a conductive surface was faster than deactivating it from a nonconductive surface.

# **Electrochemical Reversibility of the Adhesive**

To preserve catechol for repeated electrochemical reactions, a temporary protecting group in the form of phenylboronic acid, APBA, was further incorporated into the adhesive at a same concentration as DMA. ATR-FTIR spectra of the APBA-containing adhesive exhibited a new peak at 1300–1400 cm<sup>-1</sup>, which corresponded with the B-O stretching found in boronic acid (**Figure S20**)<sup>17</sup>. The adhesive property of samples that contain both APBP and DMA decreased when repeatedly exposed to 20 V for 3 min (**Figure 5a** and **Scheme S2**). The adhesion strength dropped by 90% after the application of electricity. When the polarity was reversed, adhesion strength was

recovered by using the Ag electrode as an anode for up to 3 cycles. The reduced adhesion strength was due to the formation of the catechol-boronate complex at basic pH formed by the water electrolysis around the cathode <sup>17, 18</sup>. At the recovery phase, the reverse polarity of the electrodes created a reversed pH gradient between the electrodes relative to the pH gradient that formed during the deactivation process. Thus, an acidic pH was obtained near the anodic Ag electrode and dissociated the complex formed in the adhesive. ATR-FTIR spectra confirmed the formation and disappearance of a new peak at 1494 cm<sup>-1</sup> associated with the catechol-borate complex in each deactivation and reactivation step (Figure 5b) <sup>17</sup>.



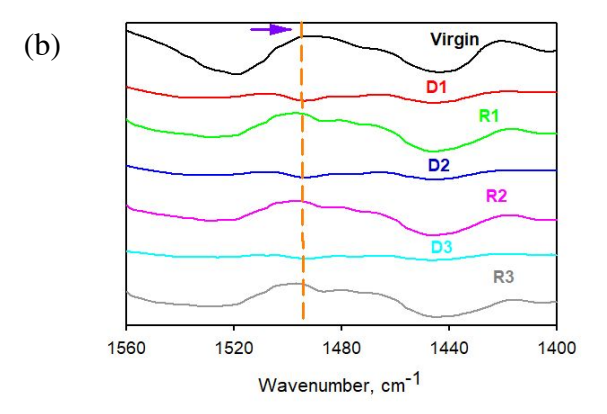


Figure 5. (a) Adhesion strength of the adhesives tested with interacting glass surface in successive contact cycles with the application of 20 V for 3 min (denoted as D) using cathodic Ag electrode for the reduction of the adhesive property and anodic Ag electrode for recovering adhesion (denoted as R). Numerical values 1–3 after D or R represent the cycle number. \* p < 0.05 when compared to the preceding contact cycle (n = 3). (b) ATR-FTIR spectra of deactivated and reactivated samples in each cycle.

Taken together, we demonstrated that it is feasible to deactivate catechol-containing adhesive from nonconductive glass and polymeric surfaces. The adhesive was coated on AM-attached PDMS, while the mesh wires were exposed to the adhesive. These exposed wires enabled the application of electricity through the adhesive without relying on the poorly conductive adhesive. The counter Ag electrode was fabricated around the adhesive's periphery to conduct electricity utilizing the ionic conductivity of water in the adhesive joint. The utilization of Ag-containing

paste was a flexible approach to fabricating the counter electrode while creating the adhesivenonconductive surface interface. This electrode configuration enabled the positioning of two electrodes across the adhesive joint without interfering with the bonding of the adhesive at the interface.

We tested various parameters that affected the process of *in situ* deactivation. Specifically, configurations that increased the level of electrical current passing through the adhesive joints (e.g., elevated voltage lever, reduced interfacial area to increase proximity to counter electrode, and increased mesh wire diameter) contributed to faster deactivation. Moreover, the deactivation process can be influenced further by modifying catechol with electron donating or withdrawing group<sup>43-47</sup>. On the contrary, using the AM-PDMS substrate has multiple advantages over a solid metal plate. The AM increased the sample's flexibility and could easily be prepared in different shapes or sizes. Also, it uses less material than an expensive metal plate while providing similar deactivating functionality. In addition, The PDMS served as a compliant backing layer, which is easily processable in various shapes or sizes, less expensive than a metal plate, and has excellent corrosion resistance properties<sup>48</sup>. PDMS is also an attractive material that can be modified to provide different properties such the incorporation of conducting additives or biopolymers<sup>49-52</sup>. However, deactivation from the nonconductive surfaces occurred at a slower rate when compared

Increasing the electronic conductivity of the adhesive by adding conductive particles or polymers may be required to speed up the deactivation process<sup>53-55</sup>. Nevertheless, the ability to deactivate catechol-based adhesives using applied electricity beyond conductive surfaces greatly increases the potential utility of this technology.

## **CONCLUSIONS**

Catechol-based smart adhesive polymerized on the AM-PDMS substrate was deactivated successfully from nonconductive glass and PMMA surfaces with applied electricity utilizing a two-electrode system. One electrode was imbedded within the adhesive while the counter electrode was coated around the periphery of the adhesive joint. This configuration enabled the passing of electrical current across the interface to deactivate the bound adhesive. The lap shear adhesion strength decreased by more than 98% when compared to the virgin adhesive. Water electrolysis initiated by the applied electricity formed a basic pH near the cathode and slowly deactivated the surface-bound adhesive via the electrochemical oxidation of catechol. Adhesive formulations that were further incorporated with phenylboronic acid demonstrated the ability to be reactivated when the polarity of the applied electricity was reversed.

## ASSOCIATED CONTENT

# **Supporting Information**

The Supporting Information is available free of charge at

treatment, and reversibility (PDF)

- The characterization of substrate and adhesive, effect of in situ electrochemical
- Video S1: Deactivation of adhesive from glass surface with 20 V (MP4)
- Video S2: *In situ* detachment of adhesive from glass surface with 20 V (MP4)
- Video S3: In situ detachment of phenol-red loaded adhesive from glass surface with 20
   V (MP4)

## **AUTHOR INFORMATION**

# **Corresponding Author**

Bruce P. Lee - Department of Biomedical Engineering, Michigan Technological University,

Houghton, Michigan 49931, United States.

Email: bplee@mtu.edu

# **Author Contributions**

The manuscript was written through contributions of all authors. All authors have given approval to the final version of the manuscript.

# **Funding Sources**

This project was supported by the Office of Naval Research under award number N00014-20-1-2230, the National Science Foundation under award numbers CMMI 2119019 and DMR 2001076, and the National Institutes of Health under award number R15GM135875.

# Notes

The authors declare no competing financial interest.

# ACKNOWLEDGMENT

The authors acknowledge Dr. Andrew Gross (Managing Director, Microfabrication Facility,

Michigan Technological University) and Machine Shop facility (Manufacturing and Mechanical

Engineering Technology, Michigan Technological University).

# **REFERENCES**

- (1) Kasprzak, K. A. Method for removing tacky adhesives and articles adhered therewith. USA U.S. Patent 4,324,595, 1982.
- (2) Dumville, J. C.; Coulthard, P.; Worthington, H. V.; Riley, P.; Patel, N.; Darcey, J.; Esposito, M.; van der Elst, M.; van Waes, O. J. Tissue adhesives for closure of surgical incisions. *Cochrane Database of Systematic Reviews* **2014**, (11), CD004287, 004281-004297. DOI: DOI: 10.1002/14651858.CD004287.pub4.
- (3) Banea, M.; Da Silva, L.; Carbas, R.; De Barros, S. Debonding on command of multimaterial adhesive joints. *The Journal of Adhesion* **2017**, *93* (10), 756-770.
- (4) Machado, J.; Nunes, P.; Marques, E.; da Silva, L. F. Adhesive joints using aluminium and CFRP substrates tested at low and high temperatures under quasi-static and impact conditions for the automotive industry. *Composites Part B: Engineering* **2019**, *158*, 102-116.
- (5) Xu, K.; Zi, P.; Ding, X. Learning from biological attachment devices: applications of bioinspired reversible adhesive methods in robotics. *Frontiers of Mechanical Engineering* **2022**, *17*(3), 1-33.
- (6) Croll, A. B.; Hosseini, N.; Bartlett, M. D. Switchable adhesives for multifunctional interfaces. *Advanced Materials Technologies* **2019**, *4*(8), 1900193.
- (7) Pinnataip, R.; Lee, B. P. Oxidation Chemistry of Catechol Utilized in Designing Stimuli-Responsive Adhesives and Antipathogenic Biomaterials. *ACS Omega* **2021**, *6*(8), 5113-5118. DOI: 10.1021/acsomega.1c00006.
- (8) Ma, Y.; Zhang, B.; Frenkel, I.; Zhang, Z.; Pei, X.; Zhou, F.; He, X. Mussel-Inspired Underwater Adhesives-from Adhesion Mechanisms to Engineering Applications: A Critical Review. *Progress in Adhesion and Adhesives* **2021**, *6*, 739-759.
- (9) Chung, H.; Glass, P.; Pothen, J. M.; Sitti, M.; Washburn, N. R. Enhanced adhesion of dopamine methacrylamide elastomers via viscoelasticity tuning. *Biomacromolecules* 2011, 12(2), 342-347.
- (10) Mian, S. A.; Gao, X.; Nagase, S.; Jang, J. Adsorption of catechol on a wet silica surface: density functional theory study. *Theoretical Chemistry Accounts* 2011, *130*, 333-339, 10.1007/s00214-011-0982-0. DOI: 10.1007/s00214-011-0982-0.
- (11) Mian, S. A.; Saha, L. C.; Jang, J.; Wang, L.; Gao, X.; Nagase, S. Density functional theory study of catechol adhesion on silica surfaces. *The Journal of Physical Chemistry C* **2010**, *114* (48), 20793-20800.

- (12) Saiz-Poseu, J.; Mancebo-Aracil, J.; Nador, F.; Busqué, F.; Ruiz-Molina, D. The chemistry behind catechol-based adhesion. *Angewandte Chemie International Edition* **2019**, *58* (3), 696-714.
- (13) Zhang, W.; Wang, R.; Sun, Z.; Zhu, X.; Zhao, Q.; Zhang, T.; Cholewinski, A.; Yang, F. K.; Zhao, B.; Pinnaratip, R. Catechol-functionalized hydrogels: biomimetic design, adhesion mechanism, and biomedical applications. *Chemical Society Reviews* 2020, 49 (2), 433-464.
- (14) Narkar, A. R.; Barker, B.; Clisch, M.; Jiang, J.; Lee, B. P. pH responsive and oxidation resistant wet adhesive based on reversible catechol–boronate complexation. *Chemistry of Materials* **2016**, *28* (15), 5432-5439.
- (15) Narkar, A. R.; Kelley, J. D.; Pinnaratip, R.; Lee, B. P. Effect of ionic functional groups on the oxidation state and interfacial binding property of catechol-based adhesive. *Biomacromolecules* **2017**, *19*(5), 1416-1424.
- (16) Narkar, A. R.; Kendrick, C.; Bellur, K.; Leftwich, T.; Zhang, Z.; Lee, B. P. Rapidly responsive smart adhesive-coated micropillars utilizing catechol–boronate complexation chemistry. *Soft matter* **2019**, *15* (27), 5474-5482.
- (17) Bhuiyan, M. S. A.; Liu, B.; Manuel, J.; Zhao, B.; Lee, B. P. Effect of Conductivity on In Situ Deactivation of Catechol–Boronate Complexation-Based Reversible Smart Adhesive. *Biomacromol.* **2021**, *22*(9), 4004-4015. DOI: 10.1021/acs.biomac.1c00802.
- (18) Akram Bhuiyan, M. S.; Roland, J. D.; Liu, B.; Reaume, M.; Zhang, Z.; Kelley, J. D.; Lee, B. P. In situ deactivation of catechol-containing adhesive using electrochemistry. *Journal of the American Chemical Society* **2020**, *142* (10), 4631-4638.
- (19) Huang, J.; Liu, Y.; Yang, Y.; Zhou, Z.; Mao, J.; Wu, T.; Liu, J.; Cai, Q.; Peng, C.; Xu, Y. Electrically programmable adhesive hydrogels for climbing robots. *Science Robotics* **2021**, *6*(53), eabe1858.
- (20) Tong, W.; Forster, M.; Dionigi, F.; Dresp, S.; Sadeghi Erami, R.; Strasser, P.; Cowan, A. J.; Farràs, P. Electrolysis of low-grade and saline surface water. *Nature Energy* 2020, 5 (5), 367-377.
- (21) Dong, Z.-H.; Jiang, Z.; Tang, T.; Yao, Z.-C.; Xue, D.; Niu, S.; Zhang, J.; Hu, J.-S. Rational design of integrated electrodes for advancing high-rate alkaline electrolytic hydrogen production. *Journal of Materials Chemistry A* **2022**, *10* (24), 12764-12787.

- (22) Zhang, H.; Bian, C.; Jackson, J. K.; Khademolhosseini, F.; Burt, H. M.; Chiao, M. Fabrication of robust hydrogel coatings on polydimethylsiloxane substrates using micropillar anchor structures with chemical surface modification. *ACS applied materials & interfaces* **2014**, *6* (12), 9126-9133.
- (23) Yue, Z.; Che, Y.; Jin, Z.; Wang, S.; Ma, Q.; Zhang, Q.; Tan, Y.; Meng, F. A facile method to fabricate thermo-and pH-sensitive hydrogels with good mechanical performance based on poly (ethylene glycol) methyl ether methacrylate and acrylic acid as a potential drug carriers. *Journal of Biomaterials Science, Polymer Edition* **2019**, *30* (15), 1375-1398.
- (24) Karan, S.; Kircelli, B. H.; Tasdelen, B. Enamel surface roughness after debonding: comparison of two different burs. *The Angle Orthodontist* **2010**, *80* (6), 1081-1088.
- (25) Yong, Q.; Chang, J.; Liu, Q.; Jiang, F.; Wei, D.; Li, H. Matt polyurethane coating: correlation of surface roughness on measurement length and gloss. *Polymers* **2020**, *12* (2), 326.
- (26) Hertz, H. The contact of elastic solids. J Reine Angew, Math 1881, 92, 156-171.
- (27) Kumar, V.; Ko, U. H.; Zhou, Y.; Hoque, J.; Arya, G.; Varghese, S. Microengineered Materials with Self-Healing Features for Soft Robotics. *Advanced Intelligent Systems* **2021**, *3*(7), 2100005.
- (28) Narkar, A. R.; Lee, B. P. Incorporation of anionic monomer to tune the reversible catechol–boronate complex for pH-responsive, reversible adhesion. *Langmuir* **2018**, *34* (32), 9410-9417.
- (29) Liu, Y.; Zhu, H.; Watanabe, A.; Yamamoto, S.; Miyashita, T.; Mitsuishi, M. Flexible ultraviolet detector with robust ZnO nanoparticle nanoassemblies on catechol-functionalized polysiloxane nanofilms. *Journal of Applied Polymer Science* **2021**, *138* (37), 50947.
- (30) Moulay, S. Dopa/catechol-tethered polymers: Bioadhesives and biomimetic adhesive materials. *Polymer Reviews* **2014**, *54*(3), 436-513.
- (31) Zoratto, N.; Matricardi, P. Semi-IPNs and IPN-based hydrogels. *Polymeric Gels* **2018**, 91-124.
- (32) Ma, J.; Zhang, L.; Fan, B.; Xu, Y.; Liang, B. A novel sodium carboxymethylcellulose/poly (N-isopropylacrylamide)/Clay semi-IPN nanocomposite hydrogel with improved response rate and mechanical properties. *Journal of Polymer Science Part B: Polymer Physics* **2008**, *46* (15), 1546-1555.

- (33) Park, K. H.; Lee, D. Y.; Yoon, S. H.; Kim, S. H.; Han, M. S.; Jeon, S.; Kim, Y.; Lim, Y. K.; Hwang, D.-H.; Jung, S.-H. Adhesion Improvement of Solvent-Free Pressure-Sensitive Adhesives by Semi-IPN Using Polyurethanes and Acrylic Polymers. *Polymers* **2022**, *14* (19), 3963.
- (34) Wang, D.; Yang, F.; Cong, L.; Feng, W.; Wang, C.; Chu, F.; Nan, J.; Chen, R. Lignin-containing hydrogel matrices with enhanced adhesion and toughness for all-hydrogel supercapacitors. *Chemical Engineering Journal* **2022**, *450*, 138025.
- (35) Li, J.; Celiz, A.; Yang, J.; Yang, Q.; Wamala, I.; Whyte, W.; Seo, B.; Vasilyev, N.; Vlassak, J.; Suo, Z. Tough adhesives for diverse wet surfaces. *Science* **2017**, *357* (6349), 378-381.
- (36) Lin, S.; Londono, C. D.; Zheng, D.; Zhao, X. An Extreme Toughening Mechanism for Soft Materials. *arXiv preprint arXiv:2202.06186* **2022**.
- (37) Han, L.; Yan, L.; Wang, K.; Fang, L.; Zhang, H.; Tang, Y.; Ding, Y.; Weng, L.-T.; Xu, J.; Weng, J. Tough, self-healable and tissue-adhesive hydrogel with tunable multifunctionality. *NPG Asia Materials* **2017**, *9*(4), e372-e372.
- (38) Kumar, D.; Singh, S. S. Static and Dynamic Mechanical Characterization of Polydimethylsiloxane (PDMS) under Uniaxial Tensile Loading. In *IOP Conference Series: Materials Science and Engineering*, 2022; IOP Publishing: Vol. 1225, p 012041.
- (39) Yang, X.; Baczyzmalski, D.; Cierpka, C.; Mutschke, G.; Eckert, K. Marangoni convection at electrogenerated hydrogen bubbles. *Physical Chemistry Chemical Physics* **2018**, *20* (17), 11542-11548.
- (40) Yuan, S.; Fan, Y.; Zhang, Y.; Tong, M.; Liao, P. Pd-catalytic in situ generation of H2O2 from H2 and O2 produced by water electrolysis for the efficient electro-Fenton degradation of rhodamine B. *Environmental science & technology* **2011**, *45* (19), 8514-8520.
- (41) Zhu, S.; So, J. H.; Mays, R.; Desai, S.; Barnes, W. R.; Pourdeyhimi, B.; Dickey, M. D. Ultrastretchable fibers with metallic conductivity using a liquid metal alloy core. *Advanced Functional Materials* **2013**, *23* (18), 2308-2314.
- (42) Kiguchi, M.; Sekiguchi, N.; Murakoshi, K. Electric conductance of metal nanowires at mechanically controllable break junctions under electrochemical potential control. *Surface science* **2007**, *601* (22), 5262-5265.

- (43) Ding, X.; Vegesna, G. K.; Meng, H.; Winter, A.; Lee, B. P. Nitro-group functionalization of dopamine and its contribution to the viscoelastic properties of catechol-containing nanocomposite hydrogels. *Macromolecular chemistry and physics* **2015**, *216* (10), 1109-1119.
- (44) Liu, B.; Li, J.; Zhang, Z.; Roland, J. D.; Lee, B. P. pH responsive antibacterial hydrogel utilizing catechol–boronate complexation chemistry. *Chemical Engineering Journal* **2022**, *441*, 135808.
- (45) Liu, B.; Zhou, C.; Zhang, Z.; Roland, J. D.; Lee, B. P. Antimicrobial property of halogenated catechols. *Chemical Engineering Journal* **2021**, *403*, 126340.
- (46) Maier, G. P.; Bernt, C. M.; Butler, A. Catechol oxidation: considerations in the design of wet adhesive materials. *Biomaterials science* **2018**, *6*(2), 332-339.
- (47) Zhang, J.; Cheah, Y. S.; Santhanakrishnan, S.; Neoh, K. G.; Chai, C. L. Methoxy group substitution on catechol ring of dopamine facilitates its polymerization and formation of surface coatings. *Polymer* **2017**, *116*, 5-15.
- (48) Ariati, R.; Sales, F.; Souza, A.; Lima, R. A.; Ribeiro, J. Polydimethylsiloxane composites characterization and its applications: A review. *Polymers* **2021**, *13* (23), 4258.
- (49) Ozkan, E.; Garren, M.; Manuel, J.; Douglass, M.; Devine, R.; Mondal, A.; Kumar, A.; Ashcraft, M.; Pandey, R.; Handa, H. Superhydrophobic and Conductive Foams with Antifouling and Oil–Water Separation Properties. *ACS Applied Materials & Interfaces* **2023**, *15* (5), 7610-7626.
- (50) Karimi-Chaleshtori, R.; Nassajpour-Esfahani, A.; Saeri, M.; Rezai, P.; Doostmohammadi, A. Silver nanowire-embedded PDMS with high electrical conductivity: nanowires synthesis, composite processing and electrical analysis. *Materials Today Chemistry* 2021, 21, 100496.
- (51) Hassouneh, S. S.; Yu, L.; Skov, A. L.; Daugaard, A. E. Soft and flexible conductive PDMS/MWCNT composites. *Journal of Applied Polymer Science* **2017**, *134* (18).
- (52) Zhang, B.; Ying, Y.; Zhu, Y.; Jiang, Y.; Zhang, Y.; Qiu, Y. Interfacial engineering in PDMS/graphene composites via anchoring polypyrrole nanowires to enhance its electrophoto thermal performance. *Carbon* **2021**, *174*, 10-23.
- (53) Deng, J.; Yuk, H.; Wu, J.; Varela, C. E.; Chen, X.; Roche, E. T.; Guo, C. F.; Zhao, X. Electrical bioadhesive interface for bioelectronics. *Nature Materials* **2021**, *20* (2), 229-236.

- (54) Li, M.; Liang, Y.; He, J.; Zhang, H.; Guo, B. Two-pronged strategy of biomechanically active and biochemically multifunctional hydrogel wound dressing to accelerate wound closure and wound healing. *Chemistry of Materials* **2020**, *32* (23), 9937-9953.
- (55) Gan, D.; Shuai, T.; Wang, X.; Huang, Z.; Ren, F.; Fang, L.; Wang, K.; Xie, C.; Lu, X. Mussel-inspired redox-active and hydrophilic conductive polymer nanoparticles for adhesive hydrogel bioelectronics. *Nano-micro letters* **2020**, *12*(1), 1-16.

# Table of Contents graphic

